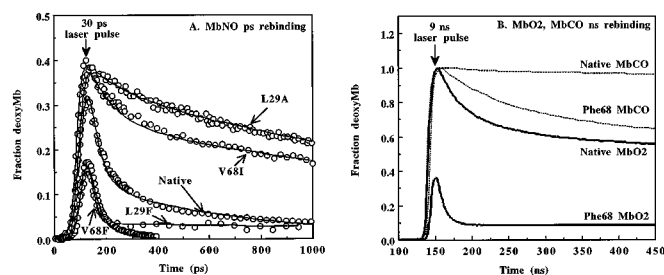


FIG. 1. Schematic structural interpretation of geminate recombination of O₂ to mammalian myoglobin under physiological conditions. Upper left, the heme pocket structure of MbO₂ showing the hydrogen bond between the distal histidine and the bound ligand. Upper right, geminate intermediates showing O₂ in the "B" state position observed by x-ray crystallography for photodissociated CO at 20 K (Fig. 5, left). As the time after photolysis increases, the pentacoordinate iron atom moves out of the plane of the pyrrole nitrogens and the ligand begins to migrate to other positions in the distal pocket. Lower left, proposed pathways for ligand escape from the distal pocket. Transient upward movement of the imidazole side chain of His-64(E7) creates a direct channel to the solvent between the heme propionates. Alternatively, the ligand may migrate to the solvent through hydrophobic channels in the protein interior. Lower right, equilibrium structure of deoxymyoglobin containing pentacoordinate, out-of-plane iron and a water molecule hydrogen bonded to the distal histidine.



an ~80% reduction in the quantum yield of photodissociated states.

The structural origin of the room temperature Mb* species and its relevance to thermal dissociation and association processes remain unclear. Petrich *et al.* (1991) examined changes in heme coordination geometry using molecular dynamics simulations. They reported that, within 1–2 ps after photolysis, the iron atom moves out of the plane of the pyrrole nitrogen atoms and takes a position very similar to that found at equilibrium. Additional fluctuations appear to occur in the next 10–1000 ps, but these are minor. Similar results were obtained in molecular dynamics simulations carried out by Gibson *et al.* (1992). These analyses suggest that the ultrafast (100 fs to 2 ps) phases may represent O₂ and NO rebinding to thermally excited, in-plane, five-coordinate heme. CO is too inert to recombine before the iron atom relaxes to its less reactive, out-of-plane position. However, this interpretation is tentative.

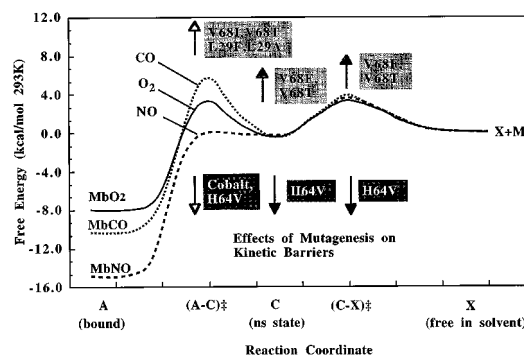


FIG. 3. Free energy barrier diagrams showing the effects of ligand chemistry, metal substitution, and mutations at positions 29(B10), 64(E7), and 68(E11). Computation of barrier heights and wells for the mutants are given in Carver *et al.* (1990) (H64V), Smerdon *et al.* (1991) (V68T), Gibson *et al.* (1992) (L29A, L29F), and Quillin *et al.* (1995) (cobalt, V68I, V68F).

Initial Movement of Dissociated Ligands (10–500 ps)

Three lines of indirect evidence have suggested that dissociated ligands initially move toward the interior of the protein molecule (Fig. 1). First, Sassaroli and Rousseau (1986) used molecular dynamics simulations to show that there is an energy minimum when dissociated CO moves into the cavity circumscribed by Leu-29(B10), Leu-32(B13), Phe-43(CD1), Val-68(E11), and Ile-107(G8) (Fig. 4, upper left panel). More sophisticated simulations of NO rebinding to wild-type and mutant myoglobins have come to a similar conclusion (Gibson *et al.*, 1992). Second, the side chain carbon atoms of covalently bound ethyl isocyanide are located in this pocket, which is presumably the sterically most accessible space (Fig. 4, lower left panel). Carver *et al.* (1990) argued that the ethyl isocyanide complex of myoglobin serves as a model for the initial trajectory of the diatomic gases with the C=N atoms mimicking the position of bound O₂, NO, and CO and the CH₃CH₂-group representing the major position of diatomic ligands in picosecond and nanosecond intermediates. Third, these interpretations are supported by the effects of distal pocket substitutions on picosecond time courses for NO rebinding (*e.g.* Carver *et al.*, 1990; Gibson *et al.*, 1992; Petrich *et al.*, 1994; Quillin *et al.*, 1995).

These proposals have been verified by the structure of the initial photoproduct for MbCO, which was determined by x-ray crystallography at 20 K (Schlichting *et al.*, 1994; Teng *et al.*, 1994) (Fig. 5, middle). There appears to be a recoil of the ligand after photolysis causing the CO molecule to move ~2 Å away from the iron atom toward the protein interior. It lies parallel to the heme plane in a position very similar to that of the alkyl side chain in ethyl isocyanide-myoglobin and that of the non-covalently bound water molecule in the distal pocket of deoxymyoglobin (Fig. 4, bottom and Fig. 5, right). In room temperature experiments using polarized excitation and IR detection, Lim *et al.* (1995b) have also shown that CO is rotated ~90° in the initial photoproduct relative to its position in the equilibrium bound state.

The Innermost Kinetic Barriers (10–500 ps)

The effects of mutagenesis, the structure of the MbCO photoproduct, and molecular dynamics simulations have suggested that picosecond recombination is governed primarily by quantum mechanical restrictions that determine ligand reactivity, secondarily by distal pocket features that enhance or restrict ligand movement, and thirdly by proximal effects that govern the reactivity and/or accessibility of the iron atom. Rapid NO recombination can be achieved in three ways: 1) increasing the reactivity of the metal atom by replacing iron with cobalt (Ikeda-Saito *et al.*, 1993); 2) inhibiting ligand movement away from the iron atom by placing phenylalanine or tryptophan diffusional barriers at positions 29 and 68; and 3) removing steric restrictions directly adjacent to the iron atom by replacing His-64 and Val-68 with smaller residues (Carlson *et al.*, 1994). The latter experiments suggest that His-64(E7) and perhaps Val-68(E11) push the ligand toward the back of the distal pocket immediately after photolysis. This steric hindrance effect is enhanced markedly when Val-68(E11) is replaced with Ile. (Fig. 2A, V68I trace, and Fig. 3) (Quillin *et al.*, 1995).

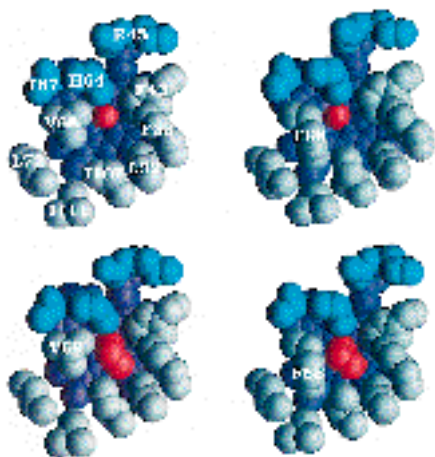


FIG. 4. Distal pocket structures of wild-type and V68F mutants of sperm whale myoglobin. The view is looking down onto the heme from the B helix (see Fig. 1). The heme group is shown in dark purple underneath the protein residues. Amino acids at the solvent interface are shown in light blue, and those in the protein interior are shown in gray. Bound CO and ethyl isocyanide are shown in red. Upper left, wild-type MbCO (Quillin *et al.*, 1993); upper right, V68F MbCO (Quillin *et al.*, 1995); lower left, wild-type Mb-ethyl isocyanide (Eich *et al.*, 1996); and lower right, V68F Mb-ethyl isocyanide (R. D. Smith, unpublished data).

The photodissociated ligand is forced to take a position parallel to the heme plane by the C- δ atoms of the Leu-29(B10) side chain. If hindrance at this position is increased by replacing Leu-29(B10) with Phe, most of the ligands reflect back immediately to the iron atom, and NO rebinding is extremely rapid (Fig. 2A, *L29F trace*). A similar phenomenon occurs when the “free” space in the distal pocket is reduced by substituting Phe for Val-68(E11) (Fig. 2A, *V68F trace*, and Fig. 4, right panels). If the distal pocket volume is increased, as in Val-29 and Ala-29 mutants, the photodissociated ligand has greater rotational and translational freedom, and NO rebinding is slower (Fig. 2A, *L29A trace*) (Gibson *et al.*, 1992).

The Nanosecond Intermediate (0.5–500 ns)

The initial picosecond movements and locations of photodissociated ligands in myoglobin are well established by experiment and theory. What happens on longer time scales is less clear. Frauenfelder and co-workers initially suggested that the nanosecond phases at room temperature represent the rebinding of ligands from positions located quite far from the iron in what was termed the protein “matrix” (see Frauenfelder *et al.*, 1988 or Ansari *et al.*, 1994). However, we have argued for a more defined ligand location.

First, the speed and extent of nanosecond geminate recombination is affected greatly by the ratio of the size of the ligand to the accessible free space on the distal side of the heme group. If this ratio is increased, much more geminate recombination occurs. For example, the fraction of nanosecond recombination is ~ 0.50 , ~ 0.80 , and ~ 0.95 for the O₂, methyl isocyanide, and ethyl isocyanide complexes, respectively, of native sperm whale myoglobin (Carver *et al.*, 1990). As shown in Fig. 4, lower left, the alkyl side chain of ethyl isocyanide prevents movement of the isocyanide group away from the active site, keeping it poised to react with the iron atom for a long time after photolysis. Large nanosecond recombination phases are observed for all ligands when the interior volume of the distal pocket is decreased by the Val-68 to Phe mutation (Fig. 2B), presumably because the ligand molecules are forced to stay in the small pocket adjacent to the iron atom (Fig. 4, upper right).

Second, the rate and extent of nanosecond rebinding can be decreased by sterically hindering access to the iron atom. The Leu-29 \rightarrow Phe mutation is particularly informative. The large Phe-29 side chain enhances picosecond rebinding of NO by preventing initial movement away from the iron atom. However, once the ligand moves past this residue to the back of the pocket, geminate rebinding is significantly reduced on all time scales >100 ps (Fig. 2A) (Gibson *et al.*, 1992). Thus, residue 29 is clearly part of the kinetic barrier inhibiting ligand movement away from and back to the iron atom.

These kinetic and structural observations show that, even in the nanosecond intermediate, the ligand molecule is in a region close



FIG. 5. Crystal structures of wild-type MbCO (left), photodissociated Mb*CO (middle), and deoxy-Mb (right) at 20 K in the P6 form. The electron density maps ($2F_o - F_c$) were taken from Schlichting *et al.* (1994). The iron density is shown in red. The red square encloses, from left to right, bound CO, photodissociated CO, and non-coordinated distal pocket water. The iron atom is, from left to right, in the plane of the pyrrole nitrogens, partially out-of-plane, and completely out-of-plane, respectively (see Fig. 1).

enough to the iron to be affected by residues Leu-29 and Val-68. We have proposed that the dissociated ligand is rapidly moving between the position seen for photodissociated CO at cryoscopic temperatures (Fig. 5, middle) and a less ordered collection of orientations in the space surrounded by Val-68, Leu-72, Ile-111, and Ile-107. Movement between these positions appears to occur on picosecond time scales (Carlson *et al.*, 1996). On nanosecond time scales, the ligand can be pictured as “smeared” throughout the empty spaces shown in Fig. 4, upper left.

This view of the nanosecond intermediate is supported by time-resolved IR measurements of photolyzed CO in myoglobin. At room temperature, two large ν_{C-O} bands associated with photodissociated CO appear with a half-time of ~ 1 –2 ps (Lim *et al.*, 1995a, 1995b). These quickly appearing bands have been assigned to ligand in “B” states on the basis of their time of appearance at room temperature and their presence at cryoscopic temperatures (Ormos *et al.*, 1988; Braunstein *et al.*, 1993). However, these spectral features persist into the nanosecond time regime and decay simultaneously with a half-time of 100–200 ns at room temperature. Most of the absorbance intensity is converted into a band representing CO dissolved in solvent (Lim *et al.* 1995a, 1995b).

As shown in Fig. 6,¹ there are significant changes in the IR spectrum of photodissociated CO when Leu-29(B10) is replaced by Phe. Two peaks appear immediately after photolysis, but one disappears quickly, and by 10 ns only a single broad band is observed. When Val-68 is replaced with Phe, the splitting between the two narrow bands is significantly greater than that seen in the wild-type protein (Fig. 6). Regardless of exact interpretation, these time-resolved IR results show that photodissociated CO is still in contact with the B10 and E11 residues on nanosecond time scales.

Pathways for Ligand Entry and Exit

At room temperature, there are two major ways of modifying the bimolecular rate of ligand entry into myoglobin. 1) Stabilization of water in the interior of the distal pocket of deoxymyoglobin causes marked decreases in the association rate constants for all ligands (Carver *et al.*, 1990; Smerdon *et al.*, 1991). In native myoglobin, a non-coordinated water molecule is hydrogen bonded to N _{ϵ} of His-64 and located very near the iron atom (Fig. 1, lower right, and Fig. 5, right). This water molecule must be displaced before ligands can bind. 2) Modification of the free space in the distal pocket also causes marked changes in the bimolecular rate of ligand entry. For example the Val-68 \rightarrow Phe substitution decreases the size of the distal pocket causing a reduction in the rate and equilibrium constants for ligand movement into protein, whereas the Leu-29 \rightarrow Ala mutation has the opposite effect (Gibson *et al.*, 1992; Quillin *et al.*, 1995).

Although considerable, these two effects do not provide clues to the pathway for ligand exit from and entry into the distal pocket. Altering the internal water content and free distal pocket volume will affect the rate of non-covalent ligand binding regardless of the exact pathway for movement into the protein. The three-dimensional structure of myoglobin reveals no pathways or channels for O₂ entry and exit. Transient motions of the protein are required to

¹ Unpublished data on position 29 and 68 mutants of recombinant sperm whale myoglobin provided by T. A. Jackson, M. Lim, T. Li, J. S. Olson, and P. A. Anfirud.

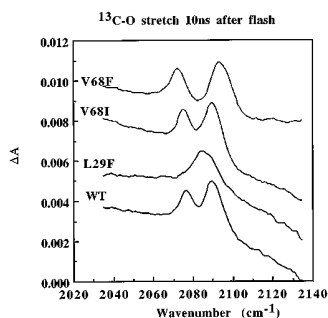


FIG. 6. IR spectra of photodissociated $^{13}\text{C-O}$ 10 ns after photolysis in three mutants and wild-type sperm whale myoglobin at room temperature, pH 7, in 70% glycerol. The experimental conditions and apparatus are described in Lim *et al.* (1995a, 1995b). These spectra represent CO in the B and C states defined in Scheme 1 and Fig. 1.¹

allow access to the iron and net dissociation to the surroundings.

Two distinct mechanisms have been proposed for ligand movement into and out of myoglobin. The first involves rotation of the side chain of His(E7) to create a direct channel from the solvent to the iron atom (see Perutz, 1989) (Fig. 1). The evidence in favor of this hypothesis includes: (a) outward displacement of His-64 in the crystal structures of the imidazole, phenylhydrazine, and ethyl isocyanide complexes of native sperm whale myoglobin (Bolognesi *et al.*, 1982; Ringe *et al.*, 1984; Johnson *et al.*, 1989); (b) increases in rates of ligand binding following protonation and outward movement of His-64 at low pH (Tian *et al.*, 1993; Yang and Phillips, 1996); and (c) increases in the rate constants for ligand entry when Phe-46 is replaced with Val or Ala causing disorder in the position of His-64 (Lai *et al.*, 1995).

The second hypothesis is that ligands enter and leave the distal pocket through several longer hydrophobic pathways between the B, G, and H helices. First proposed by Elber and Karplus (1990) on the basis of molecular dynamics simulations, this interpretation has been adopted by Huang and Boxer (1994) to explain their random mutagenesis data. In the latter experiments, point mutations at positions far removed from the distal pocket exert large effects on the rates for CO and O₂ binding. This idea is also consistent with the rate of ligand escape being roughly the same, $\sim 10^7 \text{ s}^{-1}$, for almost all of the point mutations examined so far and with the presence of multiple xenon binding sites in the interior of myoglobin (Tilton *et al.*, 1984, 1988).

Future Prospects

There is a clear need for further characterization of the ultrafast spectral intermediates seen after femtosecond photolysis of MbO₂ and MbNO. Identification of the chemical nature of these species will require the use of mutants, model compounds, time-resolved vibrational spectroscopy as well as conventional kinetic measurements, and quantum mechanical descriptions of photoexcitation and bond formation. A description of ligand movement into and out of myoglobin will require simulations on nanosecond time scales, time-resolved IR analyses of photodissociated CO in a wide variety of mutant myoglobins, and x-ray crystallographic structure determinations of nanosecond intermediates.

Perhaps the most exciting prospect is the application of these biophysical studies to the rational design of more stable and efficient O₂ delivery pharmaceuticals. Recently, Eich *et al.* (1996) have used Leu-B10 \rightarrow Phe and Val-E11 \rightarrow Phe mutations to limit NO-induced oxidation of bound O₂ in both myoglobin and hemoglobin. These substitutions were chosen because they had previously been shown to inhibit ligand entry into the distal pocket. Similar strategies are being applied to inhibit autooxidation and to enhance O₂ transport and discrimination against CO binding.

Thus, the study of myoglobin function remains an active and

important research field. In addition to providing greater understanding of the physiology of O₂ delivery, this work provides a direct connection between molecular dynamics simulations and ultrafast kinetic and structural measurements. This linkage between theory and experiment can now be used interactively to development new theoretical approaches and strategies for protein engineering.

Acknowledgments—We thank Dr. Quentin H. Gibson for reading the manuscript and making many helpful suggestions and Dr. Philip A. Anfinrud for providing the unpublished data in Fig. 6 and for expertise in describing these results.

REFERENCES

- Ansari, A., Jones, C. M., Henry, E. R., Hofrichter, J., and Eaton, W. A. (1994) *Biochemistry* **33**, 5128–5145
- Bolognesi, M., Cannillo, E., Ascenzi, P., Giacometti, G. M., Merli, A., and Brunori, M. (1982) *J. Mol. Biol.* **158**, 305–315
- Braunstein, D. P., Chu, K., Egeberg, K. D., Frauenfelder, H., Mourant, J. R., Nienhaus, G. U., Ormos, P., Sligar, S. G., Springer, B. A., and Young, R. D. (1993) *Biophys. J.* **65**, 2447–2454
- Carlson, M., Regan, R., Elber, R., Li, H., Phillips, G. N., Jr., Olson, J. S., and Gibson, Q. H. (1994) *Biochemistry* **33**, 10597–10606
- Carlson, M. L., Regan, R. M., and Gibson, Q. H. (1996) *Biochemistry* **35**, 1125–1136
- Carver, T. E., Rohlfs, R. J., Olson, J. S., Gibson, Q. H., Blackmore, R. S., Springer, B. A., and Sligar, S. G. (1990) *J. Biol. Chem.* **265**, 20007–20020
- Cornelius, P. A., Steele, A. W., Chernoff, D. A., and Hochstrasser, R. M. (1981) *Proc. Natl. Acad. Sci. U. S. A.* **78**, 7526–7529
- Eich, R. I., Li, T., Lemon, D. D., Doherty, D. H., Curry, S. R., Aitken, J. F., Mathews, A. J., Johnson, K. A., Smith, R. D., Phillips, G. N., Jr., and Olson, J. S. (1996) *Biochemistry* **35**, 6976–6983
- Elber, R., and Karplus, M. (1990) *J. Am. Chem. Soc.* **112**, 9161–9175
- Frauenfelder, H., Park, F., and Young, R. D. (1988) *Annu. Rev. Biophys. Biophys. Chem.* **17**, 451–479
- Gibson, Q. H. (1989) *J. Biol. Chem.* **264**, 20155–20158
- Gibson, Q. H., Regan, R., Elber, R., Olson, J. S., and Carver, T. E. (1992) *J. Biol. Chem.* **267**, 22022–22034
- Henry, E. R., Sommer, J. H., Hofrichter, J., and Eaton, W. A. (1983) *J. Mol. Biol.* **166**, 443–451
- Huang, X., and Boxer, S. G. (1994) *Nat. Struct. Biol.* **1**, 226–229
- Ikeda-Saito, M., Dou, Y., Yonetani, T., Olson, J. S., Li, T., Regan, R., and Gibson, Q. H. (1993) *J. Biol. Chem.* **268**, 6855–6857
- Johnson, K. A., Olson, J. S., and Phillips, G. N., Jr. (1989) *J. Mol. Biol.* **207**, 459–463
- Jongeward, K. A., Magde, D., Taube, D. J., Marsters, J. C., Traylor, T. G., and Sharma, V. S. (1988) *J. Am. Chem. Soc.* **110**, 380–387
- Lai, H. H., Li, T., Lyons, D. S., Phillips, G. N., Jr., and Olson, J. S. (1995) *Proteins Struct. Funct. Genet.* **22**, 322–339
- Lim, M., Jackson, T. A., and Anfinrud, P. A. (1995a) *J. Chem. Phys.* **102**, 4355–4366
- Lim, M., Jackson, T. A., and Anfinrud, P. A. (1995b) *Science* **269**, 962–966
- Ormos, P., Braunstein, D., Frauenfelder, H., Hong, M. K., Lin, S.-L., Sauke, T. B., and Young, R. D. (1988) *Proc. Natl. Acad. Sci. U. S. A.* **85**, 8492–8496
- Perutz, M. F. (1989) *Trends Biochem. Sci.* **14**, 42–44
- Petrich, J. W., Poyart, C., and Martin, J. L. (1988) *Biochemistry* **27**, 4049–4060
- Petrich, J. W., Lambry, J.-C., Kuczera, K., Karplus, M., Poyart, C., and Martin, J.-L. (1991) *Biochemistry* **30**, 3975–3987
- Petrich, J. W., Lambry, J.-C., Balasubramanian, S., Lambright, D. G., Boxer, S. G., and Martin, J. L. (1994) *J. Mol. Biol.* **238**, 437–444
- Quillin, M. L., Arduini, R. M., Olson, J. S., and Phillips, G. N., Jr. (1993) *J. Mol. Biol.* **234**, 140–155
- Quillin, M. L., Li, T., Olson, J. S., Phillips, G. N., Jr., Dou, Y., Ikeda-Saito, M., Elber, R., Li, H., Regan, R., and Gibson, Q. H. (1995) *J. Mol. Biol.* **245**, 416–436
- Ringe, D., Petsko, G. A., Kerr, D., and Ortiz de Montellano, P. R. (1984) *Biochemistry* **23**, 2–4
- Sassaroli, M., and Rousseau, D. L. (1986) *J. Biol. Chem.* **261**, 16292–16294
- Schlichting, I., Berendzen, J., Phillips, G. N., Jr., and Sweet, R. M. (1994) *Nature* **371**, 808–812
- Smerdon, S. J., Dodson, G. G., Wilkinson, A. J., Gibson, Q. H., Blackmore, R. S., Carver, T. E., and Olson, J. S. (1991) *Biochemistry* **30**, 6252–6260
- Springer, B. A., Sligar, S. G., Olson, J. S., and Phillips, G. N., Jr. (1994) *Chem. Rev.* **94**, 699–714
- Teng, T.-Y., Srajer, V., and Moffat, K. (1994) *Nat. Struct. Biol.* **1**, 701–705
- Tian, W. D., Sage, J. T., and Champion, P. M. (1993) *J. Mol. Biol.* **233**, 155–166
- Tilton, R. F., Jr., Kuntz, I. D., Jr., and Petsko, G. A. (1984) *Biochemistry* **23**, 2849–2857
- Tilton, R. F., Jr., Singh, U. C., Kuntz, I. D., Jr., and Kollman, P. A. (1988) *J. Mol. Biol.* **199**, 195–211
- Wald, K. N., Liu, X. Y., Sharma, V. S., and Magde, D. (1994) *Biochemistry* **33**, 2198–2209
- Yang, F., and Phillips, G. N., Jr. (1996) *J. Mol. Biol.* **256**, 762–774